Appl Nanosci (2016) 6:703–710
DOI 10.1007/s13204-015-0487-6

ORIGINAL ARTICLE

Biogenic synthesis of zinc oxide nanoparticles using *Ruta graveolens* (L.) and their antibacterial and antioxidant activities

K. Lingaraju[1] · H. Raja Naika[1] · K. Manjunath[2] · R. B. Basavaraj[3] · H. Nagabhushana[3] · G. Nagaraju[4] · D. Suresh[5]

Received: 25 April 2015 / Accepted: 5 August 2015 / Published online: 19 August 2015

Abstract In the present investigation, green synthesis of zinc oxide nanoparticles were successfully synthesized by biological method using aqueous stem extract of *Ruta graveolens* act as reducing agent. Formation of ZnO nanoparticles were characterized by powder X-ray diffraction (PXRD), UV–visible spectroscopy, scanning electron microscopy (SEM) and transmission electron microscopy (TEM) techniques. Zinc oxide nanoparticles were subjected to biological properties such as antibacterial and antioxidant studies. The PXRD pattern reveals that ZnO sample belongs to hexagonal phase with Wurtzite structure. The UV–vis absorption spectrum shows an absorption band at 355 nm due to ZnO nanoparticles. SEM images show that the particles have spherical like structure with large surface area and the average crystallite sizes were found to be in the range ~28 nm. These observations were confirmed by TEM analysis. The ZnO nanoparticles are found to inhibit the antioxidant activity of 1,1-diphenyl-2-picrylhydrazyl free radicals effectively. ZnO Nps exhibit significant bactericidal activity against Gram −ve bacterial strains such as *Klebsiella aerogenes*, *Pseudomonas aeruginosa*, *Escherichia coli* and Gram +ve *Staphylococcus aureus* by agar well diffusion method.

Keywords Antibacterial activity · Antioxidant activity · Green synthesis · ZnO nanoparticles · Room temperature

Introduction

In recent years, a rapid development of nanotechnology has opened up a world of new possibilities for fabricating nanomaterials of desired particle size, shapes suitable for uses in biomedicine, industry and agriculture field (Bhattacharya and Mukherjee 2008). Zinc oxide nanoparticles is a unique material that exhibits semiconducting, piezoelectric, and pyroelectric properties and has versatile applications in its electric and optical properties, piezoelectric devices, chemical sensors, spin electronics, personal care products, and coating and paints (Wang 2004; Wahab et al. 2010; Akhtar et al. 2011). A number of physical and chemical methods have been employed for the synthesis of ZnO nanoparticles including use of toxic chemicals (Hu et al. 2004; Zhai et al. 2008). It is believed, that broad usage of these metal oxide nanoparticles may lead to their potentially hazardous the environment which could adversely affect human health. Their possible toxicity could induce cell membrane leakage, warranting the need to develop alternative methods of environmentally benign synthesis route (Limbach et al. 2007) An eco-friendly, concerned materials like plant extract (Parashar et al. 2009), bacteria (Saifuddin and Wong 2009), fungi (Bhainsa and

Electronic supplementary material The online version of this article (doi:10.1007/s13204-015-0487-6) contains supplementary material, which is available to authorized users.

✉ H. Raja Naika
rajanaik1100@gmail.com

[1] Department of Studies and Research in Environmental Science, Tumkur University, Tumkur 572103, Karnataka, India

[2] Centre for Nano and Material Sciences, Jain University, Bangalore 562112, Karnataka, India

[3] Prof. CNR Rao Center for Advanced Materials, Tumkur University, Tumkur 572103, Karnataka, India

[4] Department of Chemistry, Siddaganga Institute of Technology, Tumkur 572103, Karnataka, India

[5] Department of Studies and Research in Chemistry, Tumkur University, Tumkur 572103, Karnataka, India

Sauza 2006) and enzymes (Willner et al. 2007) for the synthesis of silver nanoparticles offers numerous benefits of eco-friendly and compatibility for biomedical applications as they do not use toxic chemicals for the synthesis. Plant materials provide a biological synthesis route of several metallic nanoparticles which are more eco-friendly and allows a controlled synthesis with well-defined size and shape (Bar et al. 2009). Recently, synthesis of various nanoparticles using plants such as *Gloriosa superba* (Raja Naika et al. 2015), *Epigallocatechin gallate* (Suresh et al. 2015), *Manihot esculenta* (Ramasami et al. 2015), *Cinnamomum camphora* (Huang et al. 2007), *Emblica officinalis* (Ankamwar et al. 2005), lemon grass (Shankar et al. 2004) have been reported. A great deal of work has been done to investigate antimicrobial properties of ZnO NPs. Most of these studies examined the ability of ZnO to inactivate foodborne bacteria (Emamifar and Hashim 2011; Bajpai et al. 2010; Tankhiwale and Bajpai 2012).

To our knowledge little, if any, work has been done for the synthesis of ZnO NPs using aqueous stem extract of *Ruta graveolens*. *Ruta graveolens* is an odoriferous herb belonging to the family Rutaceae. *Ruta graveolens* is a well-known medicinal herb in ancient civilizations. It is used for clinical trials in many diseases such as seizure, cough, hypertension, and for wounding activities. The ingredient of *Ruta graveolens* is used in herbal veterinary medicine. In this study, we describe the use of *R. graveolens* (RG) as the reducing and stabilizing agent in the synthesis of zinc oxide nanoparticles at room temperature. The obtained ZnO nanoparticles were characterized by using PXRD, UV–visible spectroscopy, SEM, TEM, etc. Furthermore, synthesized ZnO nanoparticles were studied to evaluate their antibacterial and antioxidant properties.

Materials and methods

Materials

Ruta graveolens herbs were collected Devarayanadurga forest, near Tumkur, Karnataka, India. The herbal stem of *R. graveolens* was identified and authenticated by an herbalist from the Department of Botany, Tumkur University. All the chemicals were purchased from Sigma-Aldrich Chemicals India. The clinical isolates of bacterial strains were purchased from National Chemical Laboratory (NCL), Pune. These strains were maintained on nutrient agar slant at 4 °C.

Preparation of extract

Fresh stems of *R. graveolens* (50 g) were weighed and washed with tap water followed by distilled water to remove the dust particles. Stems of *R. graveolens* were cut into small pieces and then ground by mortar and pestle using 50 ml of de-ionized water for 10–15 min. The homogenous mixture was boiled at 60–70 °C for 30 min. After cooling, coarse filtering is employed prior to centrifuging the aqueous solution of stem extract at 4000 rpm for 30 min to remove the heavy biomass, and only the supernatant is taken. The supernatant aqueous solution was filtered by Whatman filter paper, and stored in refrigerator for further analysis.

Synthesis of nanoparticles by using the stem extract

In a 250-ml conical flask, 10 ml of *R. graveolens* (RG) stem extract is added to 90 ml of 0.1 M of zinc nitrate solution drop-wise under continuous vigorous stirring at room temperature for 4–5 h. After adding 2.0 M NaOH solution drop-wise and then continuous stirring, finally pale yellow colored solution is formed, and then incubated overnight at room temperature; white precipitate settles down at the bottom of the conical flask. This white precipitate is washed with distilled water for 2–3 times and then again washed with methanol for 3–4 times and air dried. The dried Zn-Nps were scrapped out for further analysis.

Characterization of ZnO nanoparticles

The phase identity and crystalline size of ZnO nanoparticles were characterized by Shimadzu X-ray diffractometer (PXRD-7000) with Cu-Kα radiation as source of X-rays with a wavelength $\lambda = 1.541$ Å. The UV–Vis absorption spectrum of the sample was measured on a Shimadzu UV-1800 UV–visible spectrophotometer. Morphological features were studied by scanning electron microscopy (Hitachi-7000 model) and transmission electron microscopy (Tecnaif—30 model).

Evaluation of antibacterial activity

Antibacterial activity is screened by agar well diffusion (Manjunath et al. 2014) against four bacterial strains namely Gram −ve bacteria *Klebsiella aerogenes* [NCIM-2098], *Escherichia coli* [NCIM-5051], and *Pseudomonas desmolyticum* [NCIM-2028] Gram +ve bacteria *Staphylococcus aureus* [NCIM-5022]. Nutrient agar plates are prepared and swabbed using sterile L-shaped glass rod with 100 µl of 24 h mature broth culture of individual bacterial strains. The well is made by using sterile cork borer; 6-mm wells are created into the each Petri-plate. Various concentrations of ZnO nanoparticles (200 µg and 400 µg/well) are used to assess the activity of the compound. The compound is prepared in sterile water added into the wells by using sterile micropipettes. Simultaneously the standard

antibiotics (as positive control) are tested against the pathogens. Ciprofloxacin (Hi Media, Mumbai, India) as positive control. Then the plates are incubated at 37 °C for 36 h. After the incubation period, the zone of inhibition of each well was measured and the values were noted. Triplicates were maintained in each compound and the average values are calculated for the ultimate antibacterial activity.

Evaluation of antioxidant activity

Antioxidant activity was carried out by DPPH assay using modified method of Brand-Williams (Udayabhanu et al. 2015). 1,1-Diphenyl-2-picrylhydrazyl (oxidized form) is a stable free radical with purple color. In the presence of an antioxidant which can donate an electron to DPPH radical decays, and the change in absorbance at 520 nm is followed which can be measured spectrophotometrically. 39.4 mg of DPPH is dissolved in 100 ml of methanol to get concentration of DPPH in the assay was 0.14 mM. Methanol (50 %) was prepared by diluting methanol 1:1 with de-ionized water. Ascorbic acid standard stock I (conc. 200 µg/ml) was prepared by dissolving 2 mg of ascorbic acid and make up to a volume of 10 ml with de-ionized water. For making standard graph of ascorbic acid 2, 4, 6, 8, 10 µg/ml concentration range was used. In brief, to 860 µl of 50 % methanol/ascorbic acid/test sample of various concentrations, 140 µl of 1 mM DPPH, was added, mixed and incubated at 37 °C for 30 min. The absorbance was read at 520 nm against 50 % methanol blank by spectrophotometer, a control sample was maintained without addition of the test sample. The antioxidant activity was measured with reference to the standard ascorbic acid absorbance values. The actual absorbance is taken as the absorbance difference of the control and the test sample and IC_{50} value was determined.

Results and discussion

The PXRD pattern in Fig. 1 reveals the synthesis of ZnO nanoparticles via greener route at room temperature. All the diffraction patterns were indexed to be hexagonal Wurtzite structure of ZnO Nps with lattice constants $a = 3.2417$ Å, $c = 5.1876$ Å, which are consistent with the values in standard card JCPDS 89-1397 and no indication of a secondary phase or impurity peaks were obtained. The sharp intense diffraction peaks appearing at 2θ of 31.75°, 34.40°, 36.26°, 47.53°, 56.61°, 62.90°, 67.95° and 69.06° correspond with those from (100), (002), (101), (102), (110), (103), (200), (112), and (201) orientations, respectively. The crystallite size (D) was found to be ~28 nm and was estimated from the line broadening in PXRD using Debye–Scherrer's formula (Prashantha et al. 2011)

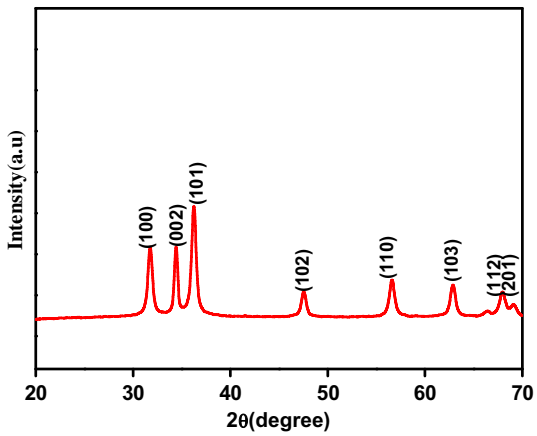

Fig. 1 PXRD patterns of ZnO Nps

$$D = \frac{K\lambda}{\beta \cos\theta}, \tag{1}$$

where D is the average crystallite size in Å, K is the shape factor (0.9), λ is the wavelength of X-ray (1.5406 Å) Cu Ka radiation, θ is the Bragg angle, and β is the full width at half maximum (FWHM).

The lattice parameters for hexagonal ZnO Nps were estimated from the relation (Chandrasekhar et al. 2012)

$$\frac{1}{d^2} = \frac{4}{3}\left[\frac{h^2 + hk + l^2}{a^2}\right] + \frac{l^2}{c^2}, \tag{2}$$

where a and c are the lattice parameters, (hkl) the Miller indices and d_{hkl} inter-planar spacing for the plane (hkl). The volume (V) of the unit cell for hexagonal system and the number of unit cells (n) in the particle (considering it to be spherical in shape) were estimated from the relations:

$$V = \frac{\sqrt{3}}{2}a^2 c \tag{3}$$

$$n = \frac{4}{3\pi\left(\frac{D}{2V}\right)}. \tag{4}$$

Significant degrees of strains were associated with nanoparticles, because they are known to have a number of surface atoms which have unsaturated co-ordinations, various structural parameters namely X-ray density (D^X), dislocation density (δ) microstrain (ε), stress and stacking fault (SF) were estimated by the following relations (Borhan et al. 2013; Sathyamoorthy et al. 2006)

$$D^X = \frac{16M}{Na^3} \tag{5}$$

$$\delta = \frac{1}{D^2} \tag{6}$$

$$\varepsilon = \frac{\beta \cos\theta}{4} \tag{7}$$

Table 1 Estimated structural parameters of ZnO NPs

Parameters	(100) plane	(002) plane	(101) plane	(102) plane	(110) plane	(103) plane	(112) plane	(201) plane
$2\theta°$	31.74	34.40	36.22	47.51	56.56	62.82	67.92	69.06
$\theta°$	15.87	17.20	18.11	23.75	28.28	31.41	33.96	34.53
$\beta \times 10^{-3}$	9.25	6.97	9.22	9.44	9.83	10.02	11.59	12.06
D (nm)	15.70	21.32	15.93	16.11	16.11	16.30	14.58	14.14
d (nm)	28.1	26.0	24.7	19.1	16.2	14.7	13.7	13.5
$n \times 10^{-22}$	25.90	21.10	25.36	25.08	25.08	24.79	27.71	28.57
$\delta \times 10^{-15}$ (kg m^{-3})	4.056	2.200	3.940	3.853	3.853	3.763	4.704	5.020
$\varepsilon \times 10^{-3}$ (kg m^{-3})$^{-2}$	2.20	1.62	2.17	2.15	2.15	2.12	2.37	2.45
$\sigma \times 10^{8}$ (Pa)	2.816	2.048	2.777	2.683	2.752	2.721	2.944	3.072
SF	0.4751	0.2276	0.2214	0.1909	0.1726	0.0731	0.1543	0.1840
$D^{X} \times 10^{4}$ (kg m^{-3}) = 6.3022 × 10^{4}								
V (Å^3) = 47.613								

$$\sigma_{\text{stress}} = \varepsilon E \tag{8}$$

$$\text{SF} = \left[\frac{2\pi^2}{45\sqrt{(3\tan\theta)}}\right], \tag{9}$$

where M molecular mass, N Avogadro's number (6.0223×10^{23} particles mol^{-1}), a lattice constant, (hkl) Miller indices, θ the Bragg's angle and E the elastic constant or generally known as Young's modulus of the material. Young's modulus of the zinc oxide is 128 GPa. The estimated structural parameters are given in Table 1.

It was noticed that the observed d-spacing of the diffraction planes were very close to the standard values and therefore the Δd_{hkl} values were very small in the order of 10–3 nm. The deviation in the d-spacing was the measure of line shifting which gives the value of microstrain in the sample. If d_0 was the observed d-spacing of the prepared sample and d_s, the spacing in the standard sample, the microstrain in the particles in the direction normal to the diffraction plane is $\Delta d_{hkl}/d_s$. If $d_0 > d_s$, then the microstrain is positive which indicates that the residual stress was tensile and if $d_0 < d_s$, microstrain was negative indicating generation of residual compressive stress in the surface. In the present study, estimated microstrain in most of the 101 plane was positive, indicating the presence of tensile stress on the surface of the particles. Observed negative values of microstrain may be due to induced error in the measurement of the 2θ value, since the respective peaks are nonsymmetrical (Suresh et al. 2013; Lima et al. 2001; Vidya et al. 2015).

FULLPROF program was used to estimate the lattice parameters for ZnO nanoparticles. Thomson–Cox–Hasting pseudo-voigt function (Premkumar et al. 2013; Young et al. 1995) was used to fit the several parameters to the data point: one scale factor, one zero shifting, four back ground, three cell parameters, five shape and width of the peaks, one global thermal factor and two asymmetric factors. The experimental and calculated PXRD pattern obtained by the Rietveld refinement is shown in Fig. 2. The line marks below the patterns represent the positions of all possible Bragg reflections. The lower solid line represents the difference between the observed and calculated intensities. In general, the Rietveld method utilizes the least-squares refinement for obtaining the best fit between the experimental data and the calculated pattern based on the simultaneously refined models. Diamond software was utilized for extracting the possible packing diagram which is shown in Fig. 3. The refined parameters such as occupancy, atomic functional positions are displayed in Table 2. The fitting parameters (R_p, R_{wp} and χ^2) indicate a good agreement between the refined and observed PXRD patterns for the hexagonal ZnO phase. The refined lattice parameters are $a = 3.2521$ Å, $c = 5.2105$ Å, unit cell volume 47.7246 Å^3 for ZnO prepared via *R. gravelones* extract, respectively. The quality of the refined data was checked by measuring goodness of fit (GOF) defined by

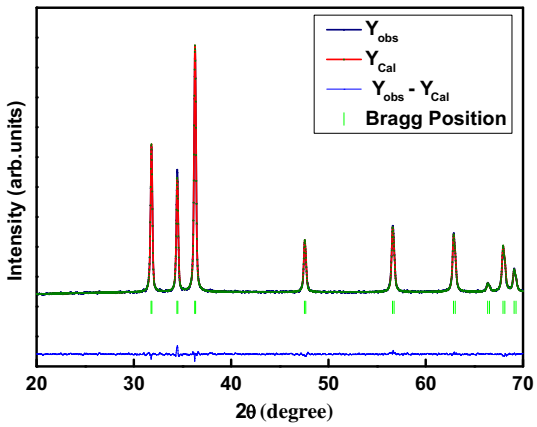

Fig. 2 Rietveld refinement of ZnO Nps

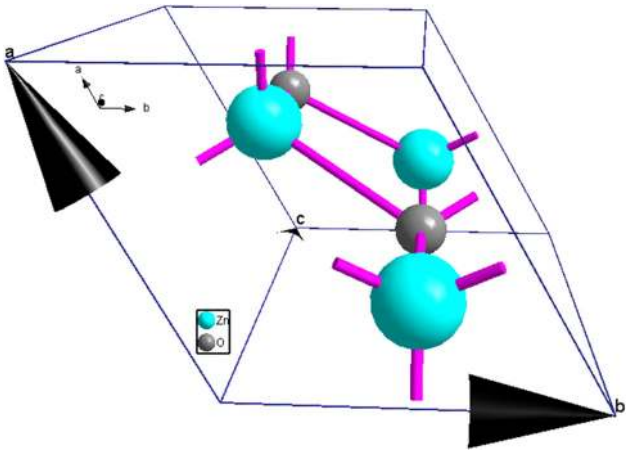

Fig. 3 Packing diagram of ZnO Nps

Table 2 Rietveld refined structural parameters of ZNPs

Crystal system	Hexagonal
Space group	P 63 m c
Hall symbol	P 6c–2c
Lattice parameters (Å)	$a = 3.2521$
	$c = 5.2105$
Unit cell volume (Å^3)	47.7246
GOF	1.143
R_p	2.75
R_{wp}	4.14
R_{exp}	3.62
χ^2	1.31
R_{Bragg}	5.50
R_F	4.06
X-ray density (g/cm^3)	5.627
Unit cell volume (Å^3)	47.7246

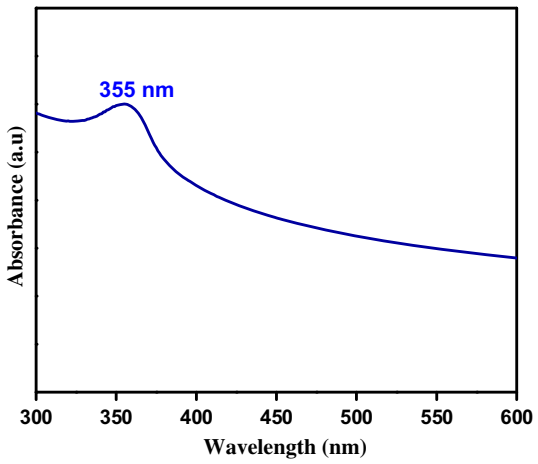

Fig. 4 UV–visible absorption spectrum of ZnO Nps

GOF = R_{wp}/R_{exp} (Jahagirdar et al. 2013; Wyckoff 1964; Klug 1954; Williamson and Hall 1953). The GOF was found to be 1.14 for the samples prepared through *R. gravelones* extract, respectively, which confirms the good fitting with experimental and theoretical plots.

Figure 4 shows the UV–visible spectrum of ZnO nanoparticles synthesized by using *R. graveolens*. The given sample exhibits a strongly broad absorption peak at 355 nm. This is due to the transfer of electrons from the valence band to the conduction band. The band gap energy corresponds to the absorption limit and can be estimated by the given relation Tauc relation (Nagabhushana et al. 2010)

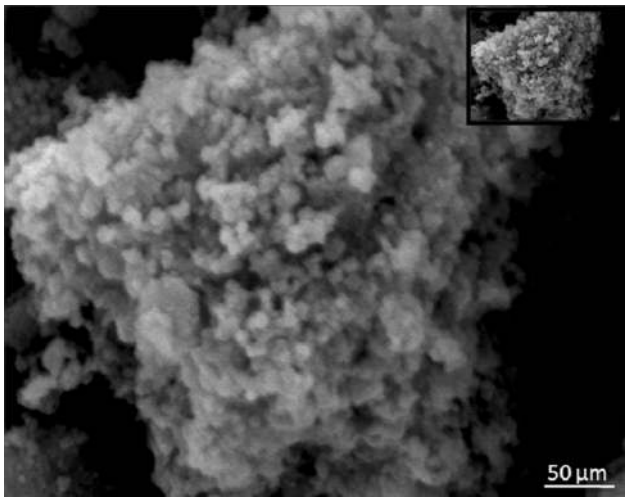

Fig. 5 SEM images of ZnO Nps

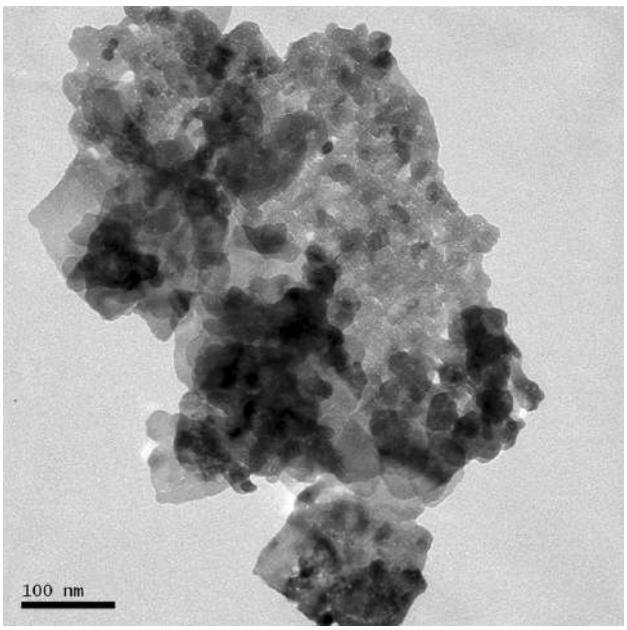

Fig. 6 TEM image of ZnO Nps

$$E_g = \frac{hC}{\lambda} \text{eV}, \quad (10)$$

where E_g is the band gap energy (eV), h is the Planck's constant (6.626×10^{-34} J s), C is the light velocity (3×10^{-8} m/s) and λ is the wavelength (nm). This is due to the transfer of electrons from the valence band to the conduction band. The estimated E_g values were found to be in the range 3.33–3.26 eV. Further, bulk ZnO has absorption band at 353 nm in the UV–visible spectrum and is superior to the as prepared ZnO nanoparticles indicating the clear blue shift (Wang et al. 2005).

The scanning electron microscopy images of the as prepared ZnO Nps are shown in Fig. 5. The images depict the formation of spherical shaped nanoparticles which are agglomerated to form cluster-like structure in the sample. The space between the particles clearly explain that the obtained sample is mesoporous.TEM micrographs show that the morphology of the ZnO nanoparticles has spherical

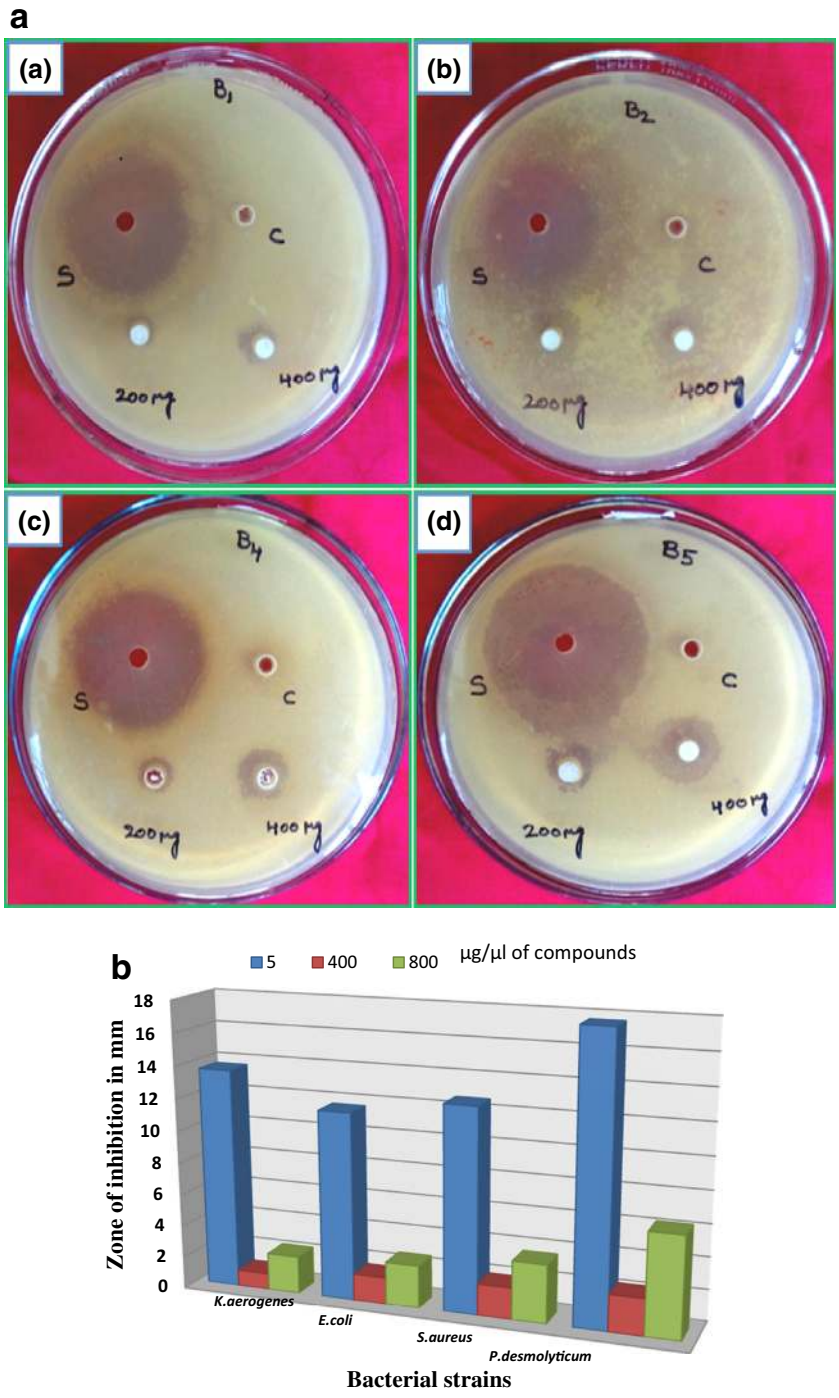

Fig. 7 **a** Antibacterial activity of ZnO Nps. **b** Graphical representation of ZnO Nps against antibacterial activity

Table 3 Antibacterial activity of ZnO nanoparticles against pathogenic bacterial strains

Treatment	*K. aerogenes* (B1) Mean ± SE	*E. coli* (B2) Mean ± SE	*S. aureus* (B4) Mean ± SE	*P. desmolyticum* (B5) Mean ± SE
Standard (5 μg/50 μL)	13.67 ± 0.03**	11.67 ± 0.09*	12.67 ± 0.06*	17.67 ± 0.12*
ZnO (200 μg/40 μL)	1.00 ± 0.00	1.67 ± 0.00	2.00 ± 0.00	2.33 ± 0.06*
ZnO (400 μg/80 μL)	2.33 ± 0.09*	2.67 ± 0.03**	3.67 ± 0.03**	6.33 ± 0.12*

Values are the mean ± SE of inhibition zone in mm

* Symbols represent statistical significance, * $P < 0.05$, ** $P < 0.01$ as compared with the control group

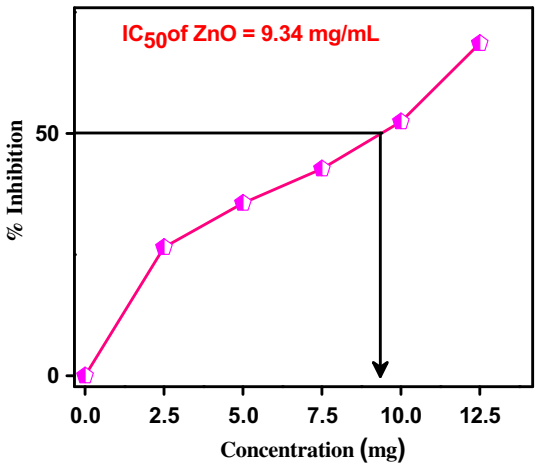

Fig. 8 Antioxidant activity of ZnO Nps

like structure with large and tiny particles with various sizes is agglomeration. The average particle size was calculated from the clearly visible particles of the TEM images with perfect boundaries and was found to be mostly in the range of 20–30 nm as shown in the Fig. 6.

Figure 7a shows the antibacterial activity of ZnO NPs was studied against Gram +ve *S. aureus* and Gram −ve *E. coli*, *K. aerogenes*, *P. desmolyticum* bacterial strains using agar well diffusion method. Significant antibacterial activity was observed against *P. desmolyticum* (6.33 ± 0.33) and moderate activity was shown against *S. aureus* (3.67 ± 0.33) *E. coli*, (2.67 ± 0.33) *K. aerogenes* (2.33 ± 0.33) with the concentration of 200 and 400 μg/μL; Table 3 shows the zone of inhibition in mm. Figure 7b shows the graphical representation of antibacterial activity of ZnO Nps against pathogenic bacterial strains. Antioxidants are micro-constituents that can be act as a scavenger of reactive oxygen species (ROS) by terminating the oxidizing chain reaction. ROS play a fundamental role in the pathogenesis of a variety of degenerative conditions including cardiovascular diseases and carcinogenesis. DPPH assay are widely used to evaluate the radical-scavenging ability of green synthesized nanoparticles. In the present study, DPPH, a stable free radical with a characteristic absorption at 517–520 nm, was used to study the radical-scavenging effects. The decrease in absorption is taken as a measure of the extent of radical scavenging. The radical-scavenging activity (RSA) values were expressed as the ratio percentage of sample absorbance decrease and the absorbance of DPPḢ solution in the absence of extract at 520 nm. The ZnO nanoparticles were proved to be inhibiting the DPPH free radical scavenging activity with IC_{50} value of 9.34 mg/ml as shown in Fig. 8. This means that it shows considerable antioxidant activity in quenching the free radical scavenging of DPPH.

Conclusion

Zinc oxide nanoparticles with well-faceted hexagonal, spherical, agglomerated particles were successfully synthesized by biological method using aqueous stem extract of *R. graveolens* as a reducing agent. The PXRD patterns confirmed single phase, hexagonal Wurtzite structure and the crystallite size was in nano-range and the same was confirmed by TEM analysis. UV–visible absorption spectrum of the as-formed ZnO Nps is blue-shifted in comparison to ZnO bulk. Significant antibacterial activity was observed on *S. aureus* and *P. demolyticum* and moderate activity on *K. aerogenes*, *E. coli*, with the concentration of 200 and 400 μg per well by agar well diffusion method. Furthermore, ZnO nanoparticles inhibit the scavenging of DPPH free radicals effectively with IC_{50} value of 9.34 mg/ml, respectively.

Acknowledgments Raja Naika thanks University Grant Commission for Major Research Project (UGC Letter No. 42-179/2013(SR) for financial assistant to carry out the research work.

References

Akhtar MS, Ameen S, Ansari SA, Yang O (2011) Synthesis, and characterization of ZnO nanorods and balls nanomaterials for dye sensitized solar cells. J Nano Eng Nano Manuf 1:71–76

Ankamwar B, Damle C, Ahmad A, Sastry M (2005) Biosynthesis of gold and silver nanoparticles using *Emblics officinalis* fruit extract and their phase transfer and transmetallation in an organic solution. J Nanosci Nanotechnol 5(10):1665–1671

Bajpai SK, Chand N, Chaurasia V (2010) Investigation of water vapor permeability and antimicrobial property of zinc oxide nanoparticles-loaded chitosan-based edible film. J Appl Polym Sci 115:674–683

Bar H, Bhui DK, Sahoo GP, Sarkar P, Pyne S, Misra A (2009) Green synthesis of silver nanoparticles using seed extract of *Jatropha curcas*. Colloids Surf: Physiochem Eng Asp 348:212–216

Bhainsa KC, Sauza SFD (2006) Extracellular biosynthesis of silver nanoparticles using the fungus *Aspergillus fumigatus*. Colloids Surf B 47:160–164

Bhattacharya R, Mukherjee P (2008) Biological properties of "naked" metal nanoparticles. Adv Drug Deliv Rev 60:1289–1306

Borhan AI, Iordan AR, Palamaru MN (2013) Correlation between structural, magnetic and electrical properties of nanocrystalline Al^{3+} substituted zinc ferrite. Mater Res Bull 48–7:2549–2556

Chandrasekhar M, Sunitha DV, Dhananjaya N, Nagabhushana H, Sharma SC, Nagabhushana BM, Shivakumara C, Chakradhar RPS (2012) Structural and phase dependent thermo and photoluminescent properties of Dy (OH) 3 and Dy 2 O 3 nanorods Mater. Resear. Bullet. 47:2085–2094

Emamifar A, Hashim A (2011) Applications of antimicrobial polymer nanocomposites in food packaging. In: Advances in nanocomposite technology, Intech, Vienna, pp 299–318

Hu XL, Zhu YJ, Wang SW (2004) Sonochemical and microwave-assisted synthesis of linked single-crystalline ZnO rod. Mater Chem Phys 88:421–426

Huang J, Li Q, Sun D, Lu Y, Su Y, Yang X, Wang H, Wang Y, Shao W, He N, Hong J, Chen C (2007) Biosynthesis of silver and gold nanoparticles by using novel sun-dried *Cinnamomum camphora* leaves. Nanotechnology 18:105104–105115

Jahagirdar AA, Dhananjaya N, Monika DL, Kesavulu CR, Nagabhushana H, Sharma SC, Nagabhushana BM, Shivakumara C, Rao JL, Chakradhar RPS (2013) Structural, EPR, optical and magnetic properties of α-Fe_2O_3 nanoparticles. Spectr Acta Part A: Mol Biomol Spectr 104:512–518

Klug P, Alexander LE (1954) X-ray diffraction procedure. Wiley, New York

Lima RS, Kucuk A, Berndt CC (2001) Evaluation of microhardness and elastic modulus of thermally sprayed nanostructured zirconia coatings. Surf Coat Technol 135(2–3):166–172

Limbach LK, Wick P, Manser P, Grass RN, Bruinink A, Stark WJ (2007) Exposure of engineered nanoparticles to human lung epithelial cells: influence of chemical composition and catalytic activity on oxidative stress. Environ Sci Technol 41:4158–4163

Manjunath K, Ravishankar TN, Kumar D, Priyanka K, Varghese T, Raja Naika H, Nagabhushana H, Sharma SC, Dupont J, Ramakrishnappa T, Nagaraju G (2014) Facile combustion synthesis of ZnO nanoparticles using *Cajanus cajan* (L.) and its multidisciplinary applications. Mater Sci Bull 57:325–334

Nagabhushana H, Nagabhushana BM, Kumar M, Premkumar HB, Shivakumara C, Chakradhar RPS (2010) Synthesis, characterization and photoluminescence properties of $CaSiO_3$:Dy^{3+} nanophosphors. Philos Mag 26:3567–3579

Parashar V, Parashar R, Sharma B, Pandey AC (2009) Parthenium leaf extract mediated synthesis silver nanoparticles: a novel approach towards weed utilization. Digest J Nanomater Biostruct 4:45–50

Prashantha SC, Lakshminarasappa BN, Nagabhushana BM (2011) Photoluminescence and thermoluminescence studies of Mg_2SiO_4:Eu^{3+} nano phosphor. J Alloys Compd 509:10185–10189

Premkumar HB, Sunitha DV, Nagabhushana H, Sharma SC, Nagabhushana BM, Shivakumara C, Rao JL, Chakradhar RPS (2013) Synthesis, characterization, EPR, photo and thermoluminescence properties of YAlO 3: Ni^{2+} nanophosphors. J Lumin 135:105–112

Raja Naika H, Lingaraju K, Manjunath K, Kumar Danith, Nagaraju G, Sureshd D, Nagabhushana H (2015) Green synthesis of CuO nanoparticles using *Gloriosasuperba* L. extract and their antibacterial activity'. J Taibah Univ Sci 9:7–12

Ramasami Alamelu K, Raja Naika H, Nagabhushana H, Ramakrishnappa T, Balakrishna GR, Nagaraju G (2015) Tapioca starch: an efficient fuel in gel-combustion synthesis of photocatalytically and anti-microbially active ZnO nanoparticles. Mater Charact 99:266–276

Saifuddin N, Wong CW, Yasumira AAN (2009) Rapid biosynthesis of silver nanoparticles using culture supernatant of bacteria with microwave irradiation. J Chem 6(1):61–70

Sathyamoorthy R, Chandramohan S, Sudhagar P, Kanjilal D, Kabiraj D, Ashokan K (2006) Structural and photoluminescence properties of swift heavy ion irradiated CdS thin films. Sol Energy Mater Sol Cells 90:2297–2304

Shankar SS, Rai A, Ankamwar B, Ahmad A, Sastry M (2004) Biological synthesis of triangular gold nanoprisms. Nat Mater 3:482–488

Suresh R, Ponnuswamy V, Mariappan R (2013) Effect of annealing temperature on the microstructural, optical and electrical properties of CeO_2 nanoparticles by chemical precipitation method. Appl Surf Sci 273:457–464

Suresh D, Udayabhanu Nethravathi PC, Lingaraju K, Raja Naika H, Sharma SC, Nagabhushana H (2015) EGCG assisted green synthesis of ZnO nanopowders photodegradative, antimicrobial and antioxidant activities. Spectr Acta Part A: Mol Biomol Spectr 136:1467–1474

Tankhiwale R, Bajpai SK (2012) Preparation, characterization and antibacterial coated polyethylene films for food packaging. Colloid Surf B 90:16–20

Udayabhanu, Nethravathi PC, Pavan Kumar MA, Suresh D, Lingaraju K, Raja Naika H, Nagabhushana H, Sharma SC (2015) *Tinospora cordifolia* mediated facile green synthesis of cupric oxide nanoparticles and their photocatalytic, antioxidant and antibacterial properties. Mater Sci Semicond Process 33:81–88

Vidya YS, Anantharaju KS, Nagabhushana H, Sharma SC, Nagaswarupa HP, Prashantha SC, Shivakumara C, Danithkumar (2015) Combustion synthesized tetragonal ZrO 2: Eu^{3+} nanophosphors: Structural and photoluminescence studies. Spectr Acta Part A: Mol Biomol Spectr 135:241–251

Wahab R, Kim YS, Lee DS, Seo JM, Shin HS (2010) Controlled synthesis of zinc oxide nanoneedles and their transformation to microflowers. Sci Adv Mater 2:424–435

Wang ZL (2004) Nanostructures of zinc oxide. Mater Today 7:26–33

Wang C, Shen E, Wang E, Gao L, Kang Z, Tian C, Lan Y, Zhang C (2005) Controllable synthesis of ZnO nanocrystals via a surfactant-assisted alcohol thermal process at a low temperature. Mater Lett 59:2867–2871

Williamson GK, Hall WH (1953) Nanoindentation study of Al356-Al_2O_3 nanocomposite prepared by ball milling. Acta Metall 1:22–31

Willner I, Basnar B, Willner B (2007) Nanoparticle-enzyme hybrid systems for nanobiotechnology. FEBS J 274:302–309

Wyckoff RWG (1964) Crystal structures. Interscience, New York, pp 4–5

Young RA, Sakthivel A, Moss TS, PaivaSantos CO (1995) DBWS-9411, an up grade of the DBWS programs for Rietveld refinement with PC and mainframe computers. J Appl Cryst 28:366–367

Zhai HJ, Wu WH, Lu F, Wang HS (2008) Effects of ammonia and CTAB on morphologies of ZnO nano-and micromaterials under solvothermal process. Mater Chem Phys 112:1024–1028